Self-Assembled 3-D Architectures of BiOBr as a Visible Light-Driven Photocatalyst

Jun Zhang,[†] Fengjun Shi,[†] Jing Lin,[†] Dongfeng Chen,[‡] Jianming Gao,[†] Zhixin Huang,[†] Xiaoxia Ding,[†] and Chengcun Tang*,[†]

College of Physical Science and Technology, Central China Normal University, Wuhan 430079, People's Republic of China, and China Institute of Atomic Energy, Beijing 102413, People's Republic of China

Received November 8, 2007. Revised Manuscript Received February 18, 2008

In this work, we demonstrated the EG-assisted solvothermal synthesis of 3-D microspherical BiOBr architectures assembled by nanosheets. The morphology and compositional characteristics of the 3-D architectures were investigated by various microscopy techniques. The possible formation mechanism for the architectures was discussed. The band gap of the obtained BiOBr materials was estimated to be 2.54 eV by UV–vis. The specific surface area and porosity of the BiOBr 3-D architectures also were investigated by using nitrogen adsorption and desorption isotherms. Because of the narrow bandgap and the novel 3-D micro-/nanostructure, the BiOBr architectures show a more excellent photocatalytic activity under visible light irradiation than the BiOBr bulk plates. Several possible reasons for the higher photocatalytic activity have been taken into consideration. In addition, the photocatalyst is stable during the reaction and can be used repeatedly.

Introduction

The photodissociation of organic compounds and/or water into hydrogen and oxygen by semiconductor photocatalysts, which is an economic and ecologically safe option for solving energy and pollution problems, has attracted intense research interest since photoelectrochemical water splitting (the Honda−Fujishima effect) was reported in 1972.[1] The thoroughly studied conventional TiO_2 system displays excellent activities and stabilities. However, it requires UV light for effective photocatalysis, thus severely rendering the overall process impractically. Therefore, the development of a visible light photocatalyst consequently has become an imperative topic in current photocatalysis research. There are two strategies to develop such photocatalysts: modification of TiO_2 (as seen in ref 2) and exploitation of novel semiconductor materials.[3]

Bibased oxyhalides have been used as selective oxidation catalysts, ionic conductors, ferroelectric materials, and pigments for many years.[4] Recently, it has been found that oxychloride (BiOCl) shows higher photocatalytic activities in degrading methyl orange (MO) as compared to TiO_2 (P25, Degussa) in the same conditions under UV light irradiation due to its layered structures and high chemical stabilities, and Bi_3O_4Cl and xBiOI-$(1 - x)$BiOCl also are efficient visible light-driven photocatalysts.[5] BiOX (X = Cl, Br, or I) compounds all crystallize in the tetragonal matlockite structure, and BiOBr is a yellow material, which means that it absorbs in the visible-light region.[6]

As known, both the size and the morphology have an influence on the properties of semiconductor oxides.[7] For photocatalysts, nanoscale materials are believed to perform better than their bulk counterparts due to the higher surface-to-volume ratio and the faster arrival to the reaction sites of the photogenerated electrons or holes. However, nanoparticles have a tendency to aggregate during aging; therefore, the active surface area decreases dramatically, and

* To whom correspondence should be addressed. Fax: 86-27-67861185; e-mail: cctang@phy.ccnu.edu.cn.
[†] Central China Normal University.
[‡] China Institute of Atomic Energy.

(1) (a) Fujishima, A.; Honda, K. *Nature (London, U.K.)* **1972**, *37*, 238. (b) Hoffmann, M. R.; Martin, S. T.; Choi, W.; Bahnemann, D. W. *Chem. Rev.* **1995**, *95*, 69. (c) Fujishima, A.; Rao, T. N.; Tryk, D. A. *J. Photochem. Photobiol., C* **2000**, *1*, 1. (d) Choi, H.; Sofranko, A. C.; Dionysiou, D. D. *Adv. Funct. Mater.* **2006**, *16*, 1067. (e) Mrowetz, M.; Selli, E. *J. Photochem. Photobiol., A* **2006**, *180*, 15.
(2) (a) Asahi, R.; Morikawa, T.; Ohwaki, T.; Aoki, K.; Taga, Y. *Science (Washington, DC, U.S.)* **2001**, *293*, 269. (b) Sakthivel, S.; Kisch, H. *Angew. Chem., Int. Ed.* **2003**, *42*, 4908. (c) Carp, O.; Huisman, C. L.; Reller, A. *Prog. Solid State Chem.* **2004**, *32*, 33. (d) Hong, X. T.; Wang, Z. P.; Cai, W. M.; Lu, F.; Zhang, J.; Yang, Y. Z.; Ma, N.; Liu, Y. J. *Chem. Mater.* **2005**, *17*, 1548.
(3) (a) Zou, Z. G.; Ye, J. H.; Sayama, K.; Arakawa, H. *Nature (London, U.K.)* **2001**, *414*, 625. (b) Kudo, A.; Kato, H.; Tsuji, I. *Chem. Lett.* **2004**, *33*, 1534. (c) Murase, T.; Irie, H.; Hashimoto, K. *J. Phys. Chem. B* **2005**, *109*, 13420. (d) Kako, T.; Zou, Z. G.; Katagiri, M.; Ye, J. H. *Chem. Mater.* **2007**, *19*, 198.
(4) (a) Francesconi, M. G.; Kirbyshire, A. L.; Greaves, C.; Richard, O.; Tendeloo, G. V. *Chem. Mater.* **1998**, *10*, 626. (b) Pfaff, G.; Reynders, P. *Chem. Rev.* **1999**, *99*, 1963. (c) Lee, J.; Zhang, Q.; Saito, F. *J. Solid State Chem.* **2001**, *160*, 469. (d) Kijima, N.; Matano, K.; Saito, M.; Oikawa, T.; Konishi, T.; Yasuda, H.; Sato, T.; Yoshimura, Y. *Appl. Catal., A* **2001**, *206*, 237. (e) Buxbaum, G.; Pfaff, G. *Industrial Inorganic Pigments*; Wiley-VCH: Weinheim, Germany, 2005.
(5) (a) Zhang, K. L.; Liu, C. M.; Huang, F. Q.; Zheng, C.; Wang, W. D. *Appl. Catal., B* **2006**, *68*, 125. (b) Lin, X. P.; Huang, T.; Huang, F. Q.; Wang, W. D.; Shi, J. L. *J. Phys. Chem. B* **2006**, *110*, 24629. (c) Wang, W. D.; Huang, F. Q.; Lin, X. P. *Scripta Mater.* **2007**, *56*, 669.
(6) (a) Sokolova, I. V.; Zakharov, V. I.; Kartuzhanskii, A. L.; Plachenov, B. T.; Sidorin, V. K. *Zh. Prikl. Spektrosk.* **1986**, *45*, 222. (b) Ketterer, J.; Kramer, V. *Acta Crystallogr., Sect. C: Cryst. Struct. Commun.* **1986**, *42*, 1098.
(7) Burda, C.; Chen, X.; Narayanan, R.; El-Sayed, M. A. *Chem. Rev.* **2005**, *105*, 1025.

10.1021/cm7031898 CCC: $40.75
Published on Web 04/08/2008

the photocatalytic activities reduce correspondingly. In addition, it is difficult to separate and recycle the nanoscale materials because of the small diameter. Therefore, considering the high-energy conversion efficiencies as well as large light-harvesting capacities and easy solid/liquid separation, micrometer 3-D architectures with nanomaterials as building blocks should have an excellent photocatalytic activity.[8]

Considering BiOBr as a possible visible light responding photocatalyst, various morphologies such as nanoparticles, nanobelts, and nanotubes have been fabricated successfully by a variety of methods.[9] However, no literature makes reference to the self-assembly of BiOBr nanoflakelet building blocks into complex micrometer 3-D ordered architectures. In this work, we report the synthesis of novel 3-D flower-like BiOBr architectures by an ethylene glycol (EG)-mediated self-assembly process.[10] The as-obtained BiOBr materials possess a fair visible light induced photocatalytic activity for the degradation of MO.

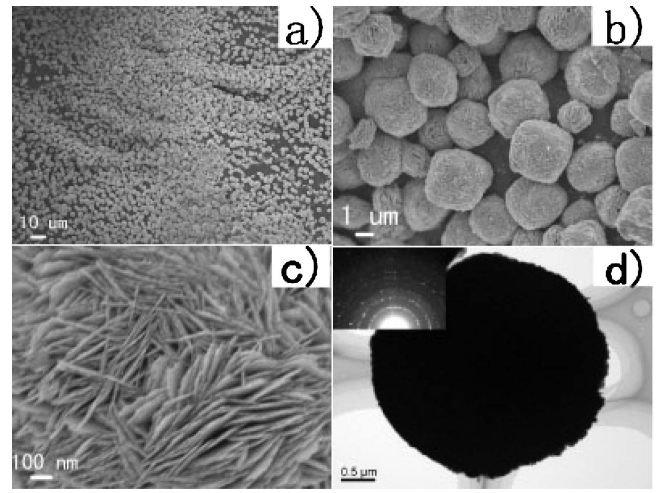

Figure 1. (a−c) SEM images of BiOBr 3-D architectures at different magnifications, (d) TEM image of a single spherical architecture, and (inset) the SAED result of the product taken from the edge of the sphere.

Experimental Procedures

Materials. All the chemicals used in this work, such as bismuth nitrate pentahydrate ($Bi(NO_3)_3 \cdot 5H_2O$), sodium bromide (NaBr), and EG were of AR grade from the Shanghai Experiment Reagent Co., Ltd. and were used without further purification.

Preparation of BiOBr 3-D Architectures. In a typical experiment, 0.73 g of $Bi(NO_3)_3 \cdot 5H_2O$ was added to 30 mL of EG with stirring at room temperature. After $Bi(NO_3)_3 \cdot 5H_2O$ was dissolved fully, 0.82 g of NaBr was added to the previous solution. Finally, a transparent solution was obtained and then transferred into a Teflon-lined stainless steel autoclave to fill 85% of the total volume. The autoclave was sealed and maintained at 170 °C for 6 h. After the reaction was completed, the autoclave was then allowed to cool naturally to room temperature, and a yellow precipitated powder was obtained. The powder was filtered and washed with deionized water several times and then dried at 60 °C for 12 h.

Preparation of BiOBr Bulk Plates. The $Bi(NO_3)_3 \cdot 5H_2O$ powders were added slowly into 100 mL of aqueous solution containing stoichiometric amounts of NaBr. The concentration of both the Bi salts and the NaBr was set to 0.05 M. Then, a 1 M $NH_3 \cdot H_2O$ solution was added dropwise into the previous mixture until the pH was adjusted to ∼4. The mixtures were stirred vigorously for 24 h. The resulting product was collected by filtration, washed several times with deionized water, and then dried at 60 °C for 12 h before further characterizations.

Characterization. The crystal structure and phase purity of the products were examined by means of X-ray diffraction (XRD) analysis with Cu Kα radiation. The overview of the sample morphology was checked by field-emission scanning electron microscopy (SEM, JSM-6700F, JEOL), in conjunction with a system of energy-dispersive spectroscopy (EDS) analysis. The sample powder was ultrasonically dispersed in acetone and dropped onto a carbon coated copper grid for a transmission electron microscopy (TEM, JEM-2010F, JEOL) measurement operating at an accelerating voltage of 200 kV. The nitrogen adsorption and desorption isotherms at 77 K were measured using a Micrometrics ASAP 2020 V3.00 H system after the sample was degassed in a vacuum at 120 °C for 400 min. Diffuse reflectance UV–vis spectra of the powders were measured at room temperature on a PE Lambda 35 spectrophotometer.

Photocatalytic Activity Measurement. The photodegradation of MO under visible light irradiation was selected to study the photocatalytic activity of BiOBr 3-D architectures. The photocatalytic system for the catalytic reaction included a 300 W Xe arc lamp, a UV cutoff filter ($\lambda > 420$ nm), and an electric fan to prevent thermal catalytic effects. Aeration was performed using an air pump to ensure a constant supply of oxygen and to complete mixing of the solution and the photocatalysts during photoreactions. In a typical photocatalytic experiment, 0.4 g of BiOBr architectures was dispersed into 400 mL of MO (10 mg/L) solutions. Visible light illumination was conducted after the suspension was strongly magnetically stirred in the dark for 20 min to reach the adsorption–desorption equilibrium of MO on the catalyst surfaces. During irradiation, ∼3 mL of the suspension continually was taken from the reaction cell at given time intervals. During the photocatalytic process, the intense yellow color of the MO solution gradually faded with increasingly longer exposure times. The photocatalyst powders and the MO solution were separated by a centrifugal machine. The MO concentration was analyzed through a UV–vis spectrophotometer (Hitachi, U-3310) by checking the absorbance at 464 nm. BiOBr plates were adopted as a reference with which to compare the photocatalytic activity under the same experimental conditions.

Results and Discussion

The morphology and structure of the product were detected by field-emission SEM and TEM, as shown in Figure 1. The low-magnification SEM image (Figure 1a) indicates that the product consists of a wealth of microspheres with diameters ranging from 3 to 7 μm. These spheres are dispersed with a good polydispersity, although most of them have discrepant

(8) (a) Zhang, L. Z.; Jimmy, C. Y. *Chem. Commun. (Cambridge, U.K.)* **2003**, 2078. (b) Zhong, L. S.; Hu, J. S.; Liang, H. P.; Cao, A. M.; Song, W. G.; Wan, L. J. *Adv. Mater.* **2006**, *18*, 2426. (c) Kale, B. B.; Baeg, J. O.; Lee, S. M.; Chang, H.; Moon, S. J.; Lee, C. W. *Adv. Funct. Mater.* **2006**, *16*, 1349. (d) Zhao, Q.; Xie, Y.; Zhang, Z.; Bai, X. *Cryst. Growth Des.* **2007**, *7*, 153.

(9) (a) Dellinger, T. M.; Braun, P. V. *Scripta Mater.* **2001**, *44*, 1893. (b) Zhu, L. Y.; Xie, Y.; Zheng, X. W.; Yin, X.; Tian, X. B. *Inorg. Chem.* **2002**, *41*, 4560. (c) Deng, H.; Wang, J. W.; Peng, Q.; Wang, X.; Li, Y. D. *Chem.—Eur. J.* **2005**, *11*, 6519. (d) Henle, J.; Simon, P.; Frenzel, A.; Scholz, S.; Kaskel, S. *Chem. Mater.* **2007**, *19*, 366.

(10) (a) Jiang, X. C.; Wang, Y. L.; Herricks, T.; Xia, Y. N. *J. Mater. Chem.* **2004**, *14*, 695. (b) Feldmann, C. *Solid State Sci.* **2005**, *7*, 868. (c) Shen, G. Z.; Chen, D.; Tang, K. B.; Liu, X. M.; Huang, L. Y.; Qian, Y. T. *J. Solid State Chem.* **2003**, *173*, 232. (d) Fievet, F.; Lagier, J. P.; Figlarz, M. *MRS Bull.* **1989**, (12), 29. (e) Shen, G. Z.; Chen, D.; Tang, K. B.; Li, F. Q.; Qian, Y. T. *Chem. Phys. Lett.* **2003**, *370*, 334. (f) Feldmann, C.; Jungk, H. O. *Angew. Chem., Int. Ed.* **2001**, *40*, 359.

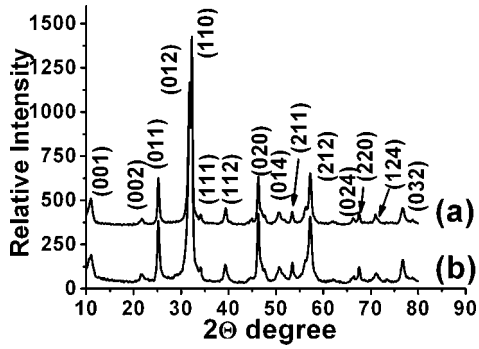

Figure 2. XRD patterns of BiOBr architectures (a) before and (b) after the photocatalytic reaction.

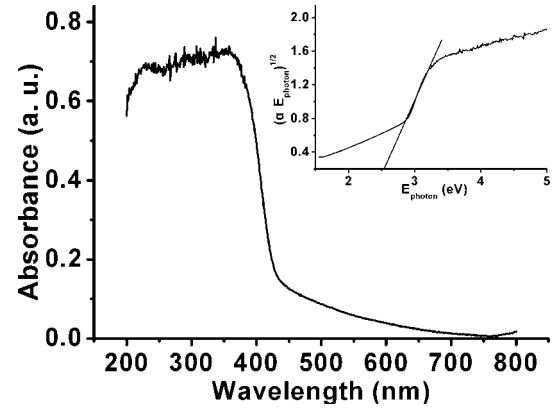

Figure 3. UV–vis diffuse reflection spectrum of the as-obtained BiOBr microsphere. The inset shows the plots of $(\alpha E_{photon})^{1/2}$ vs $\sim E_{photon}$.

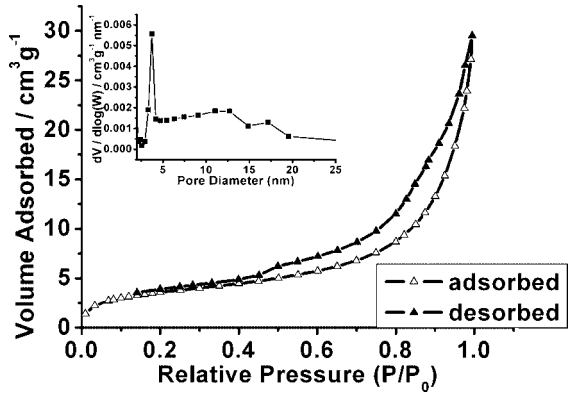

Figure 4. N_2 adsorption and desorption isotherms and pore-size distribution (inset) for the BiOBr 3-D architecture.

diameters. Under the reported conditions, the product is all in this morphology, implying that a high yield can be achieved in the adopted reaction conditions by this facile method. The exterior surfaces of the microspheres are not clearly smooth but contain an extensive growth of sheet-like structures. From the high-magnification SEM images in panels b and c of Figure 1, it can be seen that these flower-like microspheres actually are composed of many radially grown nanosheets as the petals. The thickness of these nanosheets mostly is only ~10 nm, and these nanosheets interweave together, forming an open porous structure. It should be stressed that such small sizes of these nanosheets may be indicative of a possible quantum confinement effect for the properties of such structures. TEM characterization may provide additional information regarding the interior structure of these architectures. A typical TEM image is shown in Figure 1d, which further confirms that these nanosheets are highly directed to form radial arrays from the center to the surface of these spheres. This observation suggests that the individual nanosheets were formed simultaneously and were connected together as they continued to grow. On the basis of detailed observations by TEM on many single microspheres, no distinct contrast between the edge and the center was detected, which suggests a solid structure of such architectures rather than a hollow one. A selected-area electron diffraction (SAED) pattern taken from the edge of the microsphere is shown in the inset of Figure 1d. The pattern is characterized as a transitional state from a single crystalline spot array to polycrystalline rings, indicating the single crystalline nature of the nanosheet building blocks and the presence of some ordered arrangement of such crystallites in the architectures.

The chemical composition and the phase of the obtained microspheres were confirmed with XRD and EDS. Figure 2a shows the XRD pattern of the product. All the detectable peaks in this pattern can be assigned to the tetragonal phase of BiOBr (JCPDS card no. 73-2061), displaying a high purity of the product. The narrow broadening of the peaks implies a well-crystallized BiOBr material. Consistent with the XRD results, the EDS method also reveals that the atomic ratio of Bi/O/Br in the sample is approximately equal to 1:1:1 (Figure S1 in the Supporting Information).

Regarding the formation mechanism of such 3-D spherical architectures, the layered structure of bibased oxyhalides and the EG reaction solvent may play key roles. BiOBr has a layered structure characterized by $[Bi_2O_2]$ slabs interleaved by double slabs of Br atoms,[5c,6] which results in the general formation of plate morphology. A simple array of such lamellar crystals easily will generate curvature and develop into such 3-D architectures. The curvature of the petals was further accelerated by the EG-mediated solvothermal reaction. As known, EG coordinates with metal ions to produce alkoxides, resulting in the separation of nucleation and growth. Therefore, it has been widely used as the solvent for the formation of 3-D complex architectures.[8b,11] However, the reason for such an unusual morphology is not yet well-understood, although many kinds of flower-like 3-D structures have been reported.[12] Further work is underway to investigate the details of the possible mechanism.

Diffuse reflectance spectroscopy (DRS) is a useful tool for characterizing electronic states in optical materials. The UV–vis diffuse reflectance spectrum of BiOBr spheres is shown in Figure 3. Assuming BiOBr to be an indirect semiconductor,[5] plots of $(\alpha E_{photon})^{1/2}$ versus the energy of absorbed light afforded the band gaps of BiOBr architectures

(11) (a) Cao, A. M.; Hu, J. S.; Liang, H. P.; Wan, L. J. *Angew. Chem., Int. Ed.* **2005**, *44*, 4391. (b) Yu, D. B.; Sun, X. Q.; Zou, J. W.; Wang, Z. R.; Wang, F.; Tang, K. *J. Phys. Chem. B* **2006**, *110*, 21667.

(12) (a) Xu, F.; Xie, Y.; Zhang, X.; Wu, C. Z.; Xi, W.; Hong, J.; Tian, X. B. *New J. Chem.* **2003**, *27*, 1331. (b) Wang, Z.; Qian, X. F.; Yin, J.; Zhu, Z. K. *Langmuir* **2004**, *20*, 3441. (c) Zhao, Y. P.; Ye, D. X.; Wang, G. C.; Lu, T. M. *Nano Lett.* **2002**, *2*, 351. (d) Fang, X. S.; Ye, C. H.; Zhang, L. D.; Zhang, J. X.; Zhao, J. W.; Yan, P. *Small* **2005**, *1*, 422. (e) Li, Y. B.; Bando, Y.; Golberg, D. *Appl. Phys. Lett.* **2003**, *82*, 1962.

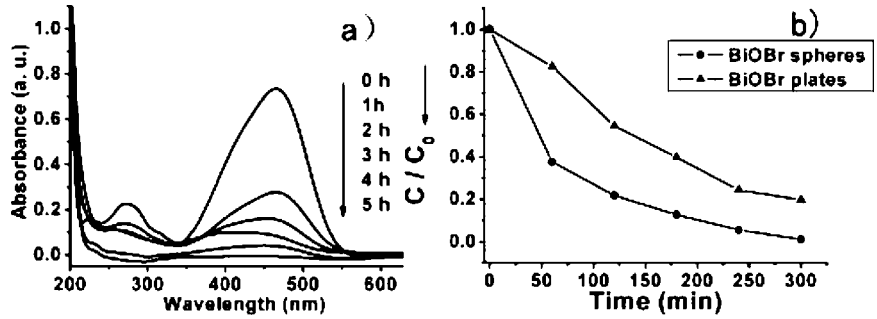

Figure 5. (a) UV–vis spectral changes of MO in aqueous BiOBr architectures as a function of visible light illumination time and (b) comparison of the photocatalytic degradation of MO in the presence of different catalysts.

as shown in the inset of Figure 3 (where α and E_{photon} are the absorption coefficient and the discrete photon energy, respectively). The extrapolated value (the straight line to the *X*-axis) of E_{photon} at $\alpha = 0$ gives an absorption edge energy corresponding to $E_g = 2.54$ eV, which is in the visible light region. It should be stressed that the steep shape of the visible edge and the strong absorption in the visible region reveal that the absorption bands of BiOBr are ascribed not to the transition from the impurity to the conduction band but to the intrinsic transition between the valence band and the conduction band.

The specific surface area and porosity of the BiOBr 3-D architectures were investigated by using nitrogen adsorption and desorption isotherms. The isotherm can be categorized as type IV with a distinct hysteresis loop observed in the range of 0.5–1.0 p/p_0, which is characteristic of mesoporous materials (Figure 4). The BET specific surface area of the sample was calculated from N_2 isotherms at 77 K and was found to be as much as $\sim$24.45 $m^2\ g^{-1}$. The powder contained small mesopores (3.7 nm) and large mesopores with maximum pore diameters of ca. 17 nm, determined by using the Barrett–Joyner–Halenda (BJH) method (inset in Figure 4). The small pores presumably arise from the nanosheets, whereas the large pores may be attributed to the internanosheet spaces.

It is well-known that porous solids have excellent adsorptive properties that possess numerous applications in catalysis and separation. Taking into account the novel 3-D architectures with nanoscale building blocks and micrometer size, also with a visible light bandgap, the as-obtained BiOBr 3-D architectures should have an excellent photocatalytic activity induced by visible light irradiation. To demonstrate the potential applicability of the present BiOBr spheres in these applications, we investigated their photocatalytic activity relative to that of the bulk plates (XRD in Figure S2) by employing the photocatalytic degradation of MO under visible light irradiation. The morphology of the bulk BiOBr was dominated by plates with thicknesses of $\sim$50 nm (Figure S3). It is well-known that MO is an acid–base model pollutant. The color of MO is determined by the azo bonds and their associated chromophores and auxochromes. Before the photocatalytic reaction, the MO solution was first photolyzed in the absence of the photocatalyst to examine its stability. The results show that MO is not decomposed even after long-time illumination of visible light. In addition, the concentration of MO almost does not change under dark conditions after the BiOBr and MO solution reaches the adsorption–desorption equilibrium. Therefore, the presence of both catalysts and illumination is necessary for efficient degradation.

Figure 5a shows the absorption spectrum of a solution of MO in the presence of 3-D BiOBr architecture under exposure to visible light for various durations in the photocatalytic degradation process. The absorption peak at $\lambda = 464$ nm diminishes gradually as the exposure time increases and completely disappears after $\sim$5 h. No new absorption bands appear in either the visible or the UV region, which indicates the complete photocatalytic degradation of MO during that reaction.[5b,13] The decoloration of the MO solution shows that the destruction of azo bonds occurs by photocatalytic reactions. The changes in the MO concentration versus the reaction time in both the BiOBr spheres and the-bulk systems are plotted, respectively, in Figure 5b, which clearly indicates that with identical visible light exposure, the 3-D architectures show a much greater activity than that of the BiOBr bulk plates. To test the stability of the BiOBr architectures during the photocatalytic process, the BiOBr spheres were reused for photocatalytic reaction 3 times under the same conditions, and we achieved the same results. Figure 2b shows the XRD pattern of BiOBr after the photocatalytic reaction, which reveals that the phase and structure remained intact. In addition, SEM investigations show no damage or change to the morphology. Thereby, the photocatalyst is stable during the reaction and can be used repeatedly.

Several reasons may account for the higher photocatalytic activity of the 3-D BiOBr spherical architectures prepared in this study as compared to the bulk one. First, it is generally accepted that the catalytic process is mainly related to the adsorption and desorption of molecules on the surface of the catalyst. The high specific surface area of the 3-D architecture (10.4 $m^2\ g^{-1}$ for bulk BiOBr) results in more unsaturated surface coordination sites exposed to the solution. The architectures with smaller and larger mesopores possess an unusual hierarchical structure. This allows more efficient transport for the reactant molecules to move to the active sites, hence enhancing the efficiency of photocatalysis. Second, the high surface-to-volume ratios of nanosheets are in favor of the transfer of electrons and holes and facilitate

(13) Lin, X. P.; Huang, F. Q.; Wang, W. D.; Wang, Y. M.; Xia, Y. J.; Shi, J. L. *Appl. Catal., A* **2006**, *313*, 218.

the degradation of MO. The prevention of the unwanted aggregation of the nanosheets fixed in the frame of architectures also is helpful in maintaining the high active surface area. In addition, the 3-D architectures have other merits, such as good dispersity and micrometer size. The good dispersity does not require constant stirring or a dark reaction for the adsorption of substrates.[14] The larger diameters of the architectures lead to the easier separation and recycling of such catalysts by means of a simple filtration step.

Conclusion

We have demonstrated for the first time the EG-assisted solvothermal synthesis of 3-D microspherical BiOBr architectures assembled by nanosheets. This method is very simple and easy to produce in a large scale. Although the growth mechanism of such BiOBr spheres is unclear, the method may be a good way to synthesize other metal oxyhalide 3-D architectures, such as BiOCl, BiOI, LnOX (X = Cl, Br, or I), etc. An excellent photocatalytic activity under visible light irradiation also was shown for the first time. Thanks to the 3-D architectures and narrow bandgap, the photocatalytic performance was significantly improved as compared to the bulk BiOBr plates. A combination of their unique features of high surface area, polydispersion, and rich stable visible light irradiated photocatalytic properties suggests that these BiOBr 3-D architectures may be found in other interesting applications in semiconductor photocatalysis, solar cells, environmental remediation, light-emitting diodes, and optoelectronic devices.

Acknowledgment. The authors gratefully acknowledge financial support for this project from the Fok Ying Tong Education Foundation (Grant 91050) and NNSF of China (Grant 50202007). Prof. Yiwen Tang and Dr. Meijuan Chen also are thanked for technical assistance with UV–vis DRS work, and Dr. Lili Ma is thanked for helpful discussions.

Supporting Information Available: EDS spectrum of BiOBr 3-D architectures and XRD pattern and SEM image of BiOBr bulk plates. This material is available free of charge via the Internet at http://pubs.acs.org.

CM7031898

(14) Hu, J. S.; Ren, L. L.; Guo, Y. G.; Liang, H. P.; Cao, A. M.; Wan, L. J.; Bai, C. L. *Angew. Chem., Int. Ed.* **2005**, *44*, 1269.